AN EXPERIMENTAL STUDY ON STRUCTURAL CHARACTERISTICS OF CANTILEVER-TYPE FOIL BEARINGS

N. Prechavut; H. P. Berg
Brandenburg University of Technology, 03046 Cottbus, Germany

Abstract

Capable of high-speed and high-temperature operation, together with an "oil-free" technology concept, gas foil bearings are a perfect solution for a novel light weight (small scale) turbo machinery. While the gas film geometry and the pressure build-up are similar to other gas lubricated bearings, and as it has been well formulated in the hydrodynamic lubrication theory, the compliant structure of the foil bearings have a variety of forms and characteristics. The cantilever-type of foil bearings are one sort of foil bearings that uses a pattern of small cantilever beams as support structure which is very robust and eases the manufacturing process. The aim of this paper is to present a measurement method and results of structural stiffness and damping characteristics of exemplary 50 mm tree-lobes radial foil bearings. Static structural test result shows that the bearing has a wide range of linear stiffness in the bearing's center area. The ramp of cartridge inner surface contour causes a cross coupling effect which may cause instability by a large rotor orbit. Increasing in bearing preload result in slightly increasing in static stiffness. In dynamic excitation test, the result shows that the dynamic stiffness is about three times higher than the static one. With a simple model of dry friction, the result shows that the dry friction coefficient is in a range of 0.4 to 0.7. The result also shows that the dynamic stiffness is more sensitive to vibration amplitude than frequency. While the damping decreases significantly with exciting frequency, especially at the vicinity of the rigid body resonance. The result evidence that the magnitude of displacement has a great effect on damping. As displacement amplitude decreases, the bearing is better in damping.

1. INTRODUCTION

Foil gas bearing is a kind of hydrodynamic gas bearing. Unlike hydrostatic bearing, hydrodynamic gas bearing requires no external pressurized gas (so called „self-acting-bearing"). Fast rotating surface of the rotor applies a shear force on a thin layer of gas and force it to flow into a small wedge shaped gap between the bearing and the rotor surface. At a certain level of speed where the hydrodynamic pressure is build-up enough to overcome the load, the rotor is separated from the bearing and glides over micrometers of gas film. After the hydrodynamic film is generated, there is no more physical contact between the rotor and bearing resulting in lower power loss, maintenance cost and noise.

Requiring only the surrounding gas, hydrodynamic gas bearings offer an "oil-free" solution for turbomachinery. Not only capable to operate at high speed and a wide range of temperature, where fluid lubricants lost their lubricating properties, without the lubrication system, hydrodynamic gas bearing also significantly reduces the weight of the machine. The oil-free technology also provides a contamination-free process which is required by some industrial applications, cabin pressurizing units in aviation industries or turbo charger in automotive market which the demand in emission standard is gradually increasing.

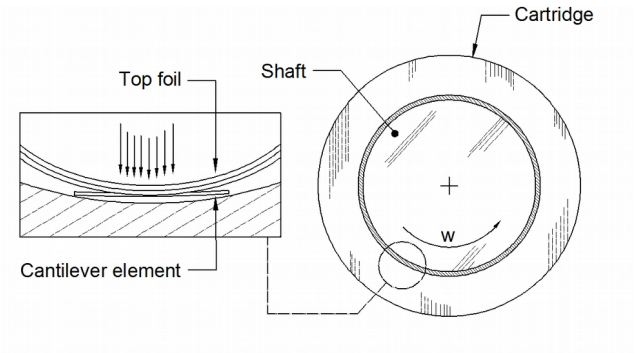

Figure 1 : A three segment foil gas bearing

Relies on a very thin lubrication gas film, the hydrodynamic gas bearings are sensitive to geometrical errors. Unlike other type of hydrodynamic gas bearing such as a tilting pad or a herring bone bearing, which have a rigid bearing surface, foil bearing has a compliant surface usually made from thin Nickel alloy sheet. Together with its spring like supporting structure, foil bearing tolerates the misalignment of the components in the machine, centrifugal growth and thermal expansion of the rotor, which is unavoidable in high range of operation temperature like gas turbines or cryogenic machines. Foil bearing also allows the designer to optimize the structural support behavior to match the working condition and to avoid instability in a selected range of operation .

Foil bearing has many designs which may roughly separated by the type of compliant structure. For instance, the well known bump-type foil bearing uses thin corrugate foil(s) as its support structure, leaf-type foil bearing which use the bending stiffness of overlapping topfoils like a leaf spring to provide resiliency. The cantilever type foil bearing use a flat form spring foil which is etched or laser cut to have small cantilever like pattern. The cantilever beam stand erect or bend out in the direction of the inner bearing cartridge surface when the spring foil is inserted into the housing as shown in Fig.1. The beam element acts like a spring support which also produces mechanical dissipation caused by the rubbing motion between the beam tips and the cartridge surface when deflected by load. The topfoil usually made of thin Nickel alloy sheet material with a certain preform radius.

A successful foil bearing application has begun since 1972 in Air-Cycle Machine (ACM) and Auxiliary power unit used on aircraft. The foil bearing ACM of 747-400 which went into production in 1988 and has shown a mean time between failure of over 100,000 hours[1]. From the past to present, the foil bearing has been further developed for better performance, reliability and operating life. Many studies and demonstrations have been done in a variety of applications such as micro gas turbine[2], turbo compressor[3], turbo charger[4], cryogenic turbo expander[5], and full scale gas turbine engines [6][7][8][9].

Motivated by the exceptional benefit of foil gas bearing, recently an example idea of foil gas bearing for automotive and aerospace application has been presented at author's institut. Fig.2 illustrates a concept of an oil free Micro Turbine with integrated Generator (MTiG) which is a compact high efficiency, electrical generator unit that enhance an “e-mobility” concept for hybrid automotive and light weight aircraft. As an example, MTiG is used as a “Power Conditioning Unit” (PCU) by an innovative, hybrid airplane to charge the battery during the flight to extend the flight duration.

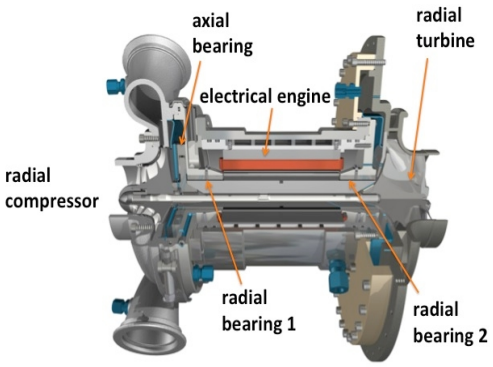

Figure 2 : MTiG Turbo generator and the positions of the air-bearings

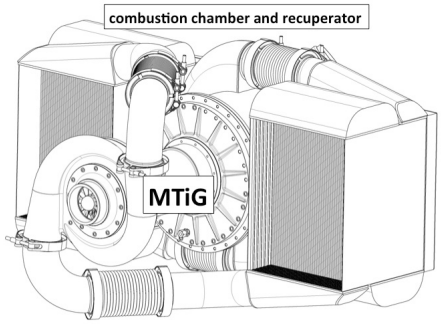

Figure 3 : MTiG Micro Turbine with Integrated Generator for innovative serial Hybrid-Aeroplanes

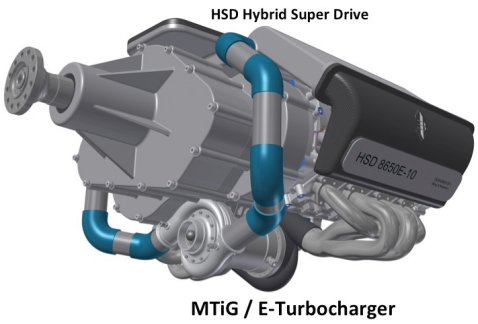

Figure 4 : Hybrid-Super Drive (HSD 8650E-10 / 858kW) for innovative Airplanes

Fig.3 shows an example of MTiG concept for a serial hybrid areoplane. In combination with an integrated generator system for power range extension (Range-Extender) or for the serial hybrid operation can be generated. The special design is also planned for future e-turbocharger, where it depends on oil free function and electrical support. An example of this is the application of an e-turbocharger configured as HSD-family concept as shown in Fig.4.

Due to the nonlinear character of hydrodynamic gas film and the supporting structure, the foil bearing design is unique in each application. Sensitive in dynamic behavior, the foil bearing has to be integrated designed from the layout process of the machine. DellaCorte[10] proposed a four step process as best practice for deploying gas bearing in a rotating machinery. Right from the feasibility study at the beginning to the rotordynamics analysis and performance optimization, the characteristic of the supporting structure of the foil bearing is the basic requirement in every design step. Understanding in the supporting structure character statically and dynamically, together with an accurate experimental data is the most important key to successful designing a high speed oil-free machine. It was found that the load capacity of the foil bearing in operation relates to its own support structure[11]. Heshmat[12] shows significant improvement of the foil bearing performance with an advance design of compliant foil structure. Due to the complicate behavior, the mathematical modeling is limited and yet cannot precisely cover all of the character of a complex geometry of supporting structures. However, with a well developed experimental process, the dynamic properties of foil bearing are disclosed and can be used as an essential asset for the foil bearing design and analysis. In additional, it can also be used for validation and improving the mathematical modeling method.

The foil bearing support structure test consist of two parts. The static force deflection test give the static stiffness of the bearing's structure which non-linearly varies with the deflection[13]. A force-deflection curve also provides information about the physical clearance, non-unifomity of the stiffness caused by the foil fixing method, maximum allowable deflection and yield point of the support structure. The dynamic excitation test is used to realize the dynamic stiffness and damping coefficient of the bearing in a function of exciting frequency, which required for rotordynamics- and instability analysis. The rate of energy dissipation can be used to estimate the structural loss factor which indicates the damping quality of the test support structure[14].

This work presents the static and dynamic test methods and results of a 50 mm three segment cantilever-type foil bearing comprise an inner cartridge ramp surface with two different shaft sizes in order to simulate the mechanical pre-load of the bearing. In static force-deflection test, the bearing cartridge is pushed against non-rotating shaft while the information of force and deflection is recorded and later calculated to determine the static stiffness. In the dynamic test, the cartridge is mounted to an electrical harmonic exciter which simulates the excitation force against the non-rotating shaft with a range of loading level and frequency. Modeled as a single degree of freedom system, the frequency response function is used to compute the dynamic stiffness and equivalent viscous damping coefficient of the bearing.

2. TEST FOIL BEARING

Based on an existing design concept[15][16], the bearing cartridge in this test has an inner contour ramp in the shaft rotating direction. The ramp form not only improves the stability of the bearing[17], but also reduces the starting torque in high preloaded bearing application. Furthermore, the rigid ramp of the cartridge ensures that the hydrodynamic wedge still exist even in the situation of high impact load where all the spring elements are flat out. The bearing has three sections separated by a foil holders which are used to hold the topfoil and the spring foil in place. To prevent the foil holder going into contact with the shaft during operation the cartridge radius at the foil holder has to be slightly larger than the smallest radius section of the bearing. For a section of bearing $\phi = 0° \text{ to } 120°$, the cartridge radius (r),measured from the center of the cartridge, varies linearly between $24° \leq \phi \leq 84°$ with difference of 60 micrometers, where the smallest radius of the bearing is at $\phi = 84°$. The annotation of ϕ and the bearing' parameters are shown in Fig.5.

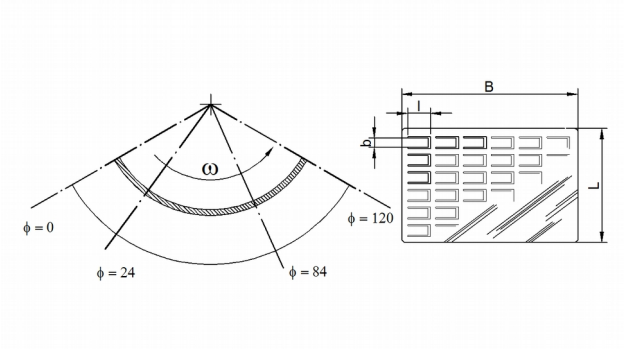

Figure 5 : Annotation of test foil bearing

Table 1: Bearing's dimensions and parameters

Dimensions and parameters		Values
Diameter of shaft-A, B [mm]	D	50.26, 50.34
Cartridge radius at 0° [mm]		25.40
Cartridge radius at 24° [mm]	r_l	25.68
Cartridge radius at 84° [mm]	r_t	25.62
Topfoil preform radius [mm]	r_p	22.00
Topfoil coating thickness [mm]	$t_{coating}$	~0.025
Top/springfoil width [mm]	B	51.40
Bearing Length	L	30.00
Top/springfoil thickness [mm]	t	0.152
Poisson' ratio	ν	0.29
Elastic Modulus [Mpa]	E	210
Bearing weight [kg]	m	0.317

Table 2: Cantilever beam length and width

Column	Beam center at ϕ	b [mm]	l [mm]
1	14°	1.904	3.211
2	21°	1.904	3.211
3	28°	2.076	3.305
4	35°	2.076	3.305
5	42°	2.353	3.396
6	49°	2.353	3.396
7	56°	2.435	3.486
8	63°	2.435	3.486
9	70°	2.621	3.572
10	77°	2.621	3.572

The topfoil is simply rolled to a radius of 22 mm. By using smaller radius, the topfoil presses against the springfoil and the cartridge when installed, ensure that the topfoil complies with the contour of the cartridge and all beam elements are in contact with cartridge inner surface. It should be noted that the preform radius of the topfoil has an effect on bearing preload which caused by the bending moment at fixing edges of the topfoil. The springfoil is chemical etched to have an array of 9 rows and 10 columns v-shape cantilever beam elements. The erect height and the stiffness of each element vary with element width (b) and beam length (l) in each column while all rows are identical. The distance between two rows is 2.8 mm. The parameters of test bearing are listed in Table 1 and Table 2.

Both top and springfoil are made out of Inconel x750 with 0.152 mm in thickness. After forming, the foils are precipitation hardened with a temperature of 704°C for 20 hours and then air cooled. To ensure an accurate test result all test parts are manufactured with +/-5 micrometers in tolerance. Both of the test shafts are polished and the topfoil surface is coated with MoS2 solid lubricant with resin binder approximately 25 micrometers in thickness in order to minimize the effect of friction between the topfoil and the shaft surface. The design of the foil bearing in this work aim to be used for experimental studies and not intend to implemented in a machine. Because of the limitation of the specification of in-house facilities, the bearing design has a length to width ratio of only 0.5 which is unusual in some applications. Without significantly large misalignment, the test result per unit area can represent the character of a bearing with higher L/D ratio.

3. EXPERIMENTAL SETUP

3.1. Static force-deflection test

Fig.6 shows the static force-deflection test setup. The non rotating shaft is fixed firmly on a rigid table with a holder block. Above the test bearing's cartridge, a piezoelectric force sensor with charge amplifier of 0.05 N/mV in sensitivity is mounted on a vertically movable sleeve. The sleeve is driven up and down along a rigid circular column with a crank handle. The fine thread of 0.5 mm per revolution allowes the sleeve to move continuously with small increment. An eddy current sensor is placed underneath the cartridge exactly on the same axis of the force sensor.

The test was performed by slowly pushing the cartridge using the vertical moving sleeve until the force reaches 400 N and then slowly release until the cartridge is back to its original position. The force and deflection signal are real-time monitored and

recorded. The test was repeated five times on ten different loading angles (ϕ) and two shafts diameters (D) . Test data are averaged and fitted with bicubic spline interpolation. The static stiffness can be obtained by using 2nd order finite differencing of $\partial f / \partial x$ of the fitted data.

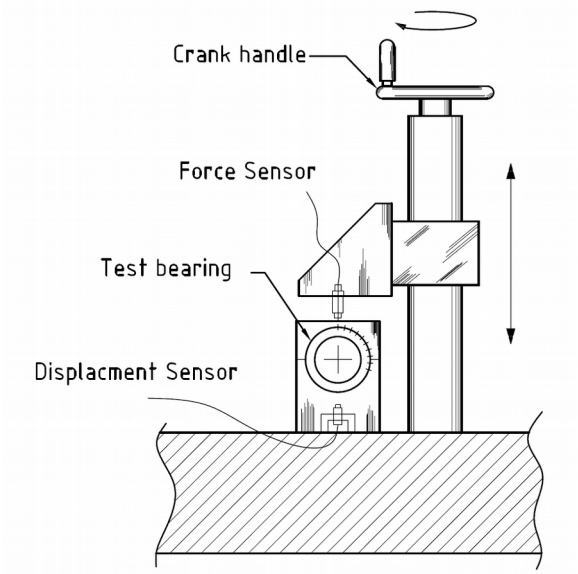

Figure 6 : Static force-deflection test setup

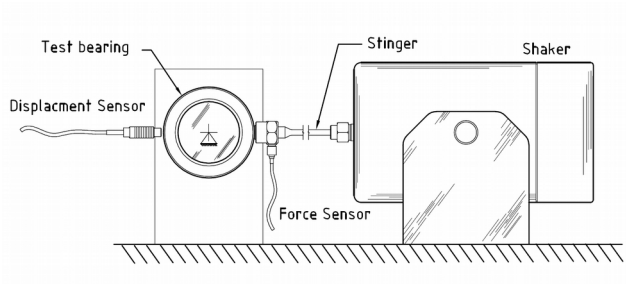

Figure 7 : Dynamic excitation test setup

3.2. Dynamic excitation test

In the dynamic excitation test, as shown in Fig.7, the shaft is held on a massive granite table in the same manner as in the static force-deflection test setup. A piezoelectric force sensor is mounted horizontally on the test bearing cartridge. On the opposite side, an eddy current sensor is positioned in the same axis of the force sensor. A stinger rod is used to connect the force sensor to a shaker which is capable to produce 31 N peak harmonic load up to 9000 Hz .

The test was performed with three different loading levels (shaker input voltage). The cartridge was excited harmonically from 50 to 600 Hz with an increment of 10 Hz and 5 second in dwell time. With a sample rate of 40 kHz, both force and deflection signal are recorded.

The test bearing is considered as a single degree of freedom system with coulomb damping[14]. The equation of motion of a system with harmonic excitation force $f(t)$ and dry friction force $F_f sgn(\dot{x})$ in a form of equivalent viscous damping can be written as

$$M\ddot{x}+K x+C_{eq}\dot{x}=f(t) \tag{1}$$

where M is the bearing mass, K is the structural stiffness coefficient and C_{eq} is the equivalent viscous damping. Corresponding to a harmonic excitation at a single frequency $f(t)=F\,\mathrm{e}^{i\omega t}$, the response is also in harmonic form $x(t)=X\,\mathrm{e}^{i\omega t}$. Thus, the equation (1) can be written in frequency domain as

$$(K+i\,\omega C_{eq}-M\,\omega^2)=\frac{F}{X} \tag{2}$$

Equation (2) is an inverse transfer function of the system which can be separated into a real and an imaginary part.

$$K=\mathrm{Re}\left(\frac{F}{X}\right)+M\,\omega^2 \tag{3}$$

$$C_{eq}=\mathrm{Im}\left(\frac{F}{X}\right)/\omega \tag{4}$$

With the Fast Fourier Transformation of input and response signal, the structural stiffness and equivalent damping coefficient can be derived from equation (3) and (4). The work done by the shaker for one period of motion is

$$W=\oint f(t)\,\dot{X}(t)dt=\pi\,F\,X\sin(theta) \tag{5}$$

The mechanical energy dissipation in a period of motion can be defined as viscous damping coefficient and dry friction force

$$E_f=\oint \dot{x}\,sgn(\dot{x})dx=4\,F_f\,X \tag{6}$$

Using energy dissipation approach, the work done by external force must be equal to energy dissipated by damping mechanism. Thus equation (5) is equal to equation (6) which gives

$$F_f=\frac{W}{4}X=\frac{-F\pi\sin(\theta)}{4} \tag{7}$$

4. RESULTS AND DISSCUSION

4.1. Static force-deflection test

In Fig.8 and Fig.9, the force-deflection curve and stiffness of the shaft-A at a loading angle of ϕ=84 ° and ϕ=24 ° , where the smallest clearance and largest clearance of the bearing are located. In Fig.8, the sudden increase in stiffness at high deflection indicates that the bearing has reached the deflection limit. As the shaft approaching the cartridge inner surface, the spring elements are flat out and no longer provide any flexibility. The maximum deflection can be estimated by $\epsilon_{max}=r(\phi)-D/2-2t-t_{coating}$, which for shaft-A, gives $\epsilon_{max}=0.221\,mm$ at ϕ=24 ° and $\epsilon_{max}=0.161\,mm$ at ϕ=84 ° . The force deflection result agree with the maximum deflection calculation on both positions. At 100 micrometers deflection on ϕ=84 ° position, the test shows an unrealistic result. As the shaft approaches the top of the ramp contour of the cartridge inner surface, due to the large deflection, the contact region has become non-symmetric to the loading axis. Thus the resultant force is deviated from the input force direction which causes the shaft to move transversely. By using only one displacement sensor aligned with the loading direction which cannot sense the change in transverse direction, cause the result of static stiffness to be inaccurate. However a wide range of linear stiffness near the bearing center is disclosed.

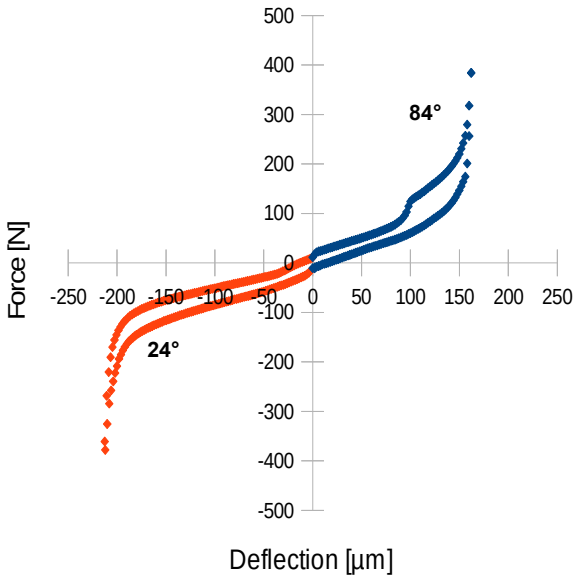

Figure 8 : Force-deflection curve

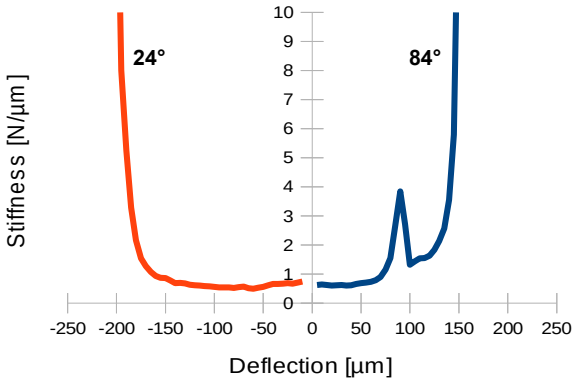

Figure 9 : Stiffness versus deflection

Fig.10 and Fig.11 confirm the uniformity of static stiffness on all directions in a range of approximately 80 micrometers of deflection. In this deflection zone, the bearing can be considered as an isotropic bearing. However, a large deflection could cause non-uniformity of the bearing and cross coupling effect which makes the bearing prone to backward whirl instability.

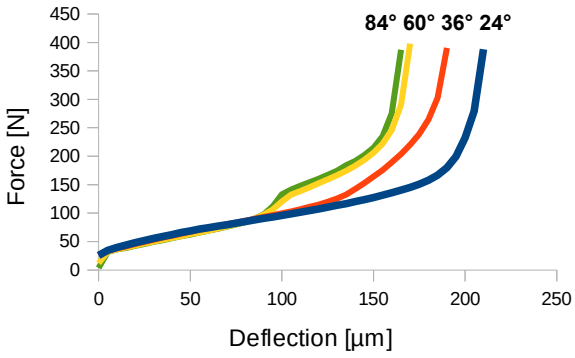

Figure 10 : Force-deflection at difference loading angle

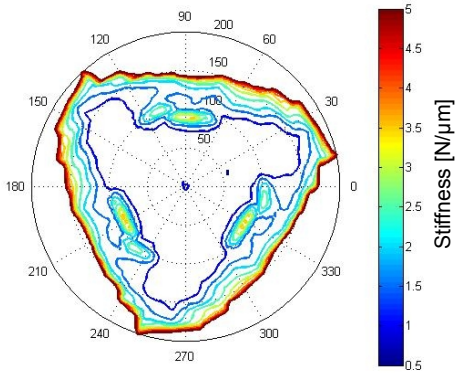

Figure 11 : Contour plot of stiffness deflection of shaft-A in polar coordinate (ϵ,ϕ)

The effect of mechanical preload can be seen in Fig.12 and Fig.13. The maximum deflection confirms the 40 micrometer of preload. The force deflection curve shows a similar trend on both shafts, except a narrower linear stiffness zone. The stiffness of higher preload bearing increases approximately by 20%, which could be a result from friction. With higher preload, the bearing still shows uniformity of stiffness in a range of 50 micrometer deflection from the shaft center, as shown in Fig.14.

The force deflection result shows a hysteresis feature caused by the coulomb friction between the cantilever element and the inner cartridge surface. It should be noted that the friction between the topfoil and shaft surface is unavoidably included due to the absence of the gas film. Slightly higher stiffness at the beginning of deflection is one of the results from the stick-slip effect between the topfoil and the shaft, which would not occur when the foil bearing is in operation where the gas film separates both surfaces completely.

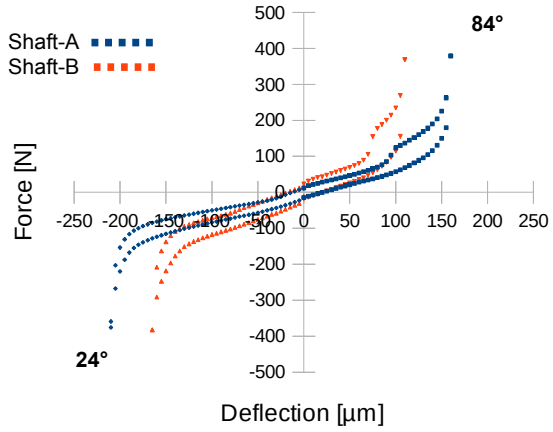

Figure 12 : Effect of higher preload on force-deflection

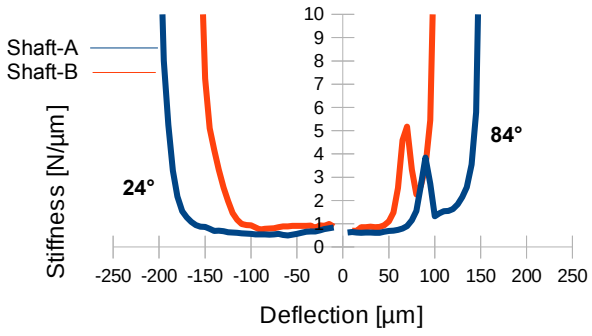

Figure 13: Effect of higher preload on stiffness

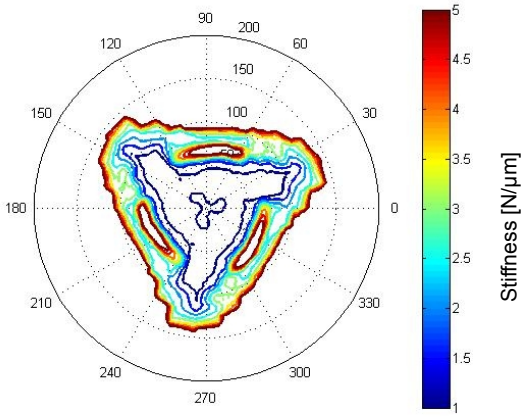

Figure 14 : Contour plot of stiffness deflection of shaft-B in polar coordinate (ϵ, ϕ)

4.2. Dynamic excitation test

At the system natural frequency the real part of frequency response function of deflection and force is equal to zero, where the inertial cancels the stiffness effect. As shown in Fig.15, regardless of loading levels, the result indicates the system natural frequency of 360 Hz. Fig.16 and Fig.17 shows the dynamic force and displacement in the frequency domain of the system at different loading level. High amplitude of force and displacement at a vicinity of 500 Hz is a result from the resonance of the shaft mounting structure and a drop of amplitude at 192 Hz is caused by the resonance of the foundation of the test bench. It should be noted that at these points the result is inaccurate.

For a typical SDOF system with damping, the maximum amplitude of displacement occurs at $\omega = \sqrt{1-2\zeta^2} * \omega_n$ where ω_n is the natural frequency. Result shows that the damping ratio ζ increases as the loading level increases. For loading level 1 to 3 (higher shaker input voltage), the damping ratios are 0.17, 0.32, and 0.44 respectively.

The dynamic stiffness has a factor about two to three times the static stiffness a relatively constant in the range of test frequency as shown in Fig.18. A small deviation between loading level is found to be related with the vibration amplitude. As shown in Fig.19, the stiffness tends to be effected from the stick-slip effect between sliding pairs including the topfoil and shaft surface, which has more influence when the vibration amplitude is particularly small.

Considering as a simple friction model, the friction coefficient can be estimated by using $\mu = F_f / F$. As shown in Fig.20, the friction coefficient at a frequency range of 50 Hz to 250 Hz varies between 0.4 to 0.7 which is a typical range for dry friction among metals. Close to natural frequency as mentioned in[14], the simple model of friction gives unrealistic value.

Damping, as shown in Fig.21, decreases gradually when exciting frequency increases. The higher loading level results in lower damping in the region before natural frequency. Beyond the natural frequency, damping in different loading conditions is nearly identical.

As mentioned earlier, the result of damping around 500 Hz is not realistic due to the resonance of the other components. However, from the trend of this result together with the result presented by Rubio and San Andres [14], the damping has a tendency to become very low or even negative at higher frequency. Since foil bearing has relatively low stiffness but requiring high speed operation, all of rotors supported with foil bearings are operating over their rigid body resonance frequency. Lack of bearing damping, the rotor with foil bearing is not tolerate to rotor bending resonance. Fig.21 also shows that the damping decrease as the vibration amplitude increase, because the dry friction relates with the relative velocity of the contact pair. At the same frequency, higher vibration amplitude result in higher velocity. Limiting the rotor's orbit by mean of preloading or using stiffer supporting structure can improve the damping of the system.

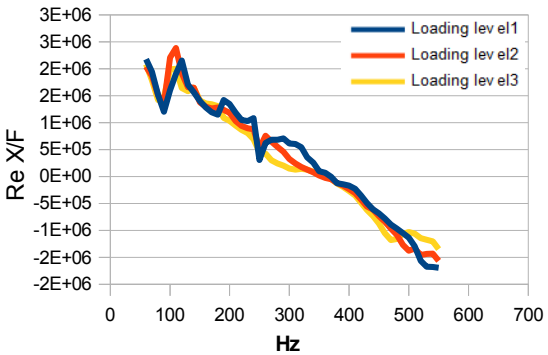

Figure 15: Real part of deflection/force FRF

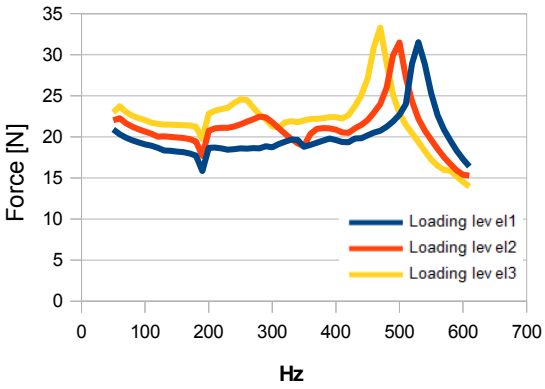

Figure 16: Excitation force on frequency domain

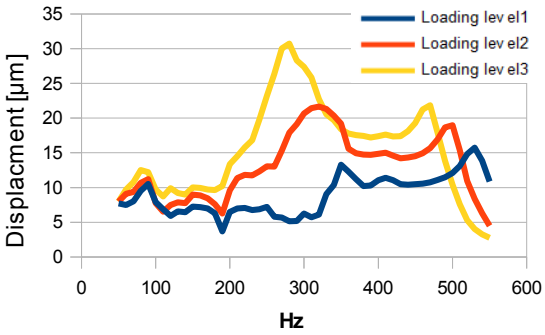

Figure 17: Displacment on frequency domain

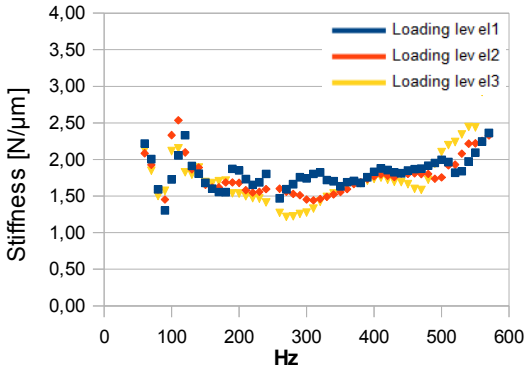

Figure 18: Stiffness over frequency

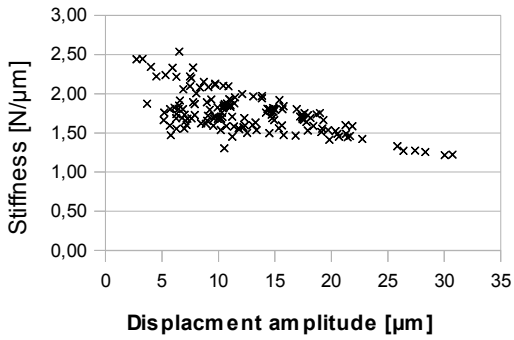

Figure 19: Stiffness vs displacment

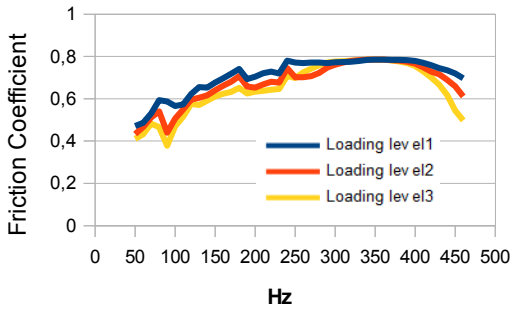

Figure 20: Friction coefficient

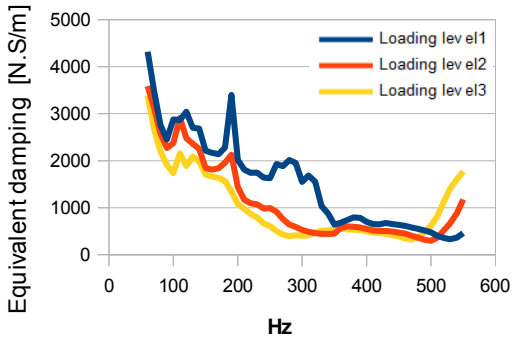

Figure 21: Damping over frequency

5. CONCLUSION

In this paper, a static force-deflection and dynamic stiffness and damping of a three lobes Cantilever type foil bearing with variate beam length and cartridge inner contour comprise a ramp in rotating direction based on existing design is presented. The test was conducted by using two non-rotating shafts which differs in diameter to simulate preloading in the bearing. The static test result shows a wide linear stiffness region near the center of the bearing. The stiffness is uniformly in all direction in the 90 micrometer deflection zone. At higher deflection, cause by the non-symmetrical shape of the cartridge inner surface, the bearing becomes anisotropic. The cross coupling term may leads to high instability when the shaft operates with large orbit. Higher preload slightly effects the bearing stiffness but the direction independent character of static stiffness is still presence. In the dynamic excitation test, the bearing cartridge is excited by electronic shaker with three different loading levels from 50 Hz to 600 Hz. By using the real part of the frequency response function of deflection and force, the natural frequency of the system is found at 360 Hz. The result shows that the dynamic stiffness is more related to displacement amplitude than frequency. On the other hand, the damping coefficient is strongly dependent to the exciting frequency. As the frequency increases, the damping decreases gradually. Furthermore, the displacement amplitude also greatly effect the damping. Higher in amplitude resulting in lower damping. Thus, limiting the shaft orbit by using higher preload or less compliant structure may improve the bearing stability.

6. REFERENCES

[1] Agrawal, Giri L., "Foil Air/Gas Bearing Technology - An Overview", ASME paper, 1997, No.97-GT347

[2] Vleugels, Peter and Waumans, Tobias and Peirs, Jan and Al-Bender, Farid and Reynaerts, Dominiek, "High-speed bearings for micro gas turbines: stability analysis of foil bearings", Journal of Micromechanics and Microengineering, 2006, Vol.16

[3] Wade, Jonathan L and Lubell, Daniel R and Weissert, Dennis, "Successful Oil-Free Version of a Gas Compressor Through Integrated Design of Foil Bearings", ASME Turbo Expo, 2008, p.969-973

[4] Lee, Yong-Bok and Park, Dong-Jin and Kim, Tae Ho and Sim, Kyuho, "Development and performance measurement of oil-free turbocharger supported on gas foil bearings", Journal of Engineering for Gas Turbines and Power, 2012, Vol.134(3)

[5] Hou, Y and Zhu, ZH and Chen, CZ, "Comparative test on two kinds of new compliant foil bearing for small cryogenic turbo-expander", Cryogenics, 2004, Vol.44(1), p.69-72

[6] K. R. Swenson, N. M. Hughes, D. F. Heuer, "Evaluation of Gas Lubricated Hydrodynamic Bearings in a Gas Turbine Environment", The Garrett Corperation : AiResearch Manufacturing Division, 1972

[7] Heshmat, Hooshang and Walton, JF and DellaCorte, Christopher and Valco, MJ, "Oil-free turbocharger demonstration paves way to gas turbine engine applications", ASME paper, 2000,2000-GT, p.620

[8] DellaCorte, Christopher and Bauman, Steven W and Radil, Kevin C and Stanford, Malcolm K and Howard, S Adam and Bruckner, Robert J, "Advanced Rotor Support Technologies for Closed Brayton Cycle Turbines", 3rd International Energy Conversion Engineering Conference, 2005, AIAA 2005-5513

[9] Howard, Samuel A and Bruckner, Robert J and DellaCorte, Christopher and Radil, Kevin C, "Preliminary Analysis for an Optimized Oil-Free Rotorcraft Engine Concept", NASA Paper, 2008, NASA/TM-2008-215064, ARL-TR-4398

[10] DellaCorte, Christopher, "Oil-Free shaft support system rotordynamics: Past, present and future challenges and opportunities", Mechanical Systems and Signal Processing, 2012, Vol.29, p.67-76

[11] DellaCorte, Christopher and Valco, Mark J, "Load capacity estimation of foil air journal bearings for oil-free turbomachinery applications", Tribology Transactions, 2000, Vol.43(4), p.795-801

[12] Heshmat, H, "Advancements in the performance of aerodynamic foil journal bearings: high speed and load capability", Journal of Tribology, 1994, Vol.116(2), p.287-294

[13] Rubio, Dario and San Andres, Luis, "Bump-type foil bearing structural stiffness: experiments and predictions", Journal of engineering for gas turbines and power, 2006, Vol.128(3), p.653-660

[14] Rubio, Dario and San Andres, Luis, "Structural Stiffness, Dry Friction Coefficient, and Equivalent Viscous Damping in a Bump-Type Foil Gas Bearing", Journal of engineering for gas turbines and power, 2007, Vol.129(2), p.494-502

[15] Robert W. Bosley, "Compliant Foil Hydrodynamic Fluid Film Radial Bearing", United States Patent, 1995,US5427455

[16] Dennis H. Weissert, "Compliant Foil Fluid Film Radial Bearing", United States Patent, 1999, US5915841

[17] Kim, Tae Ho and Andres, Luis San, "Effects of a Mechanical Preload on the Dynamic Force Response of Gas Foil Bearings: Measurements and Model Predictions", Tribology Transactions, 2009, volume52(4), p.569-580